Tremor source location using time reversal: Selecting the appropriate imaging field

C. S. Larmat,[1] R. A. Guyer,[1,2] and P. A. Johnson[1]

Received 6 August 2009; revised 29 September 2009; accepted 15 October 2009; published 21 November 2009.

[1] Studying triggered Non Volcanic Tremor (NVT) is important because it may help to map the depth of the locked zones of faults associated with high seismic risk. The success of this mapping depends on precisely locating the depth of tremor. Tremor, like other long-lived signals (e.g., Earth hum) lacks distinct sharp timing features making it impossible to locate with classical approaches. Time Reversal has the advantage of exploiting the full waveform with no a priori assumption regarding the source or the observed signal. We perform a synthetic study of time reversal location of a long-lasting source in the Los Angeles basin with a realistic 3D velocity model and sparse station set. We show that, the key to successfully locating NVT, is application of suitable imaging fields, such as the wave divergence, curl and energy current. **Citation:** Larmat, C. S., R. A. Guyer, and P. A. Johnson (2009), Tremor source location using time reversal: Selecting the appropriate imaging field, *Geophys. Res. Lett.*, *36*, L22304, doi:10.1029/2009GL040099.

1. Introduction

[2] Triangulation is often used for earthquakes source location. It relies on picking *sharp in time* features in the seismic signal. Many newly discovered seismic sources, volcanic and non-volcanic tremor, glacial "earthquakes", and hum have no sharp features in time. Consequently ad hoc approaches have been developed including cross correlation between recording stations in combination with triangulation [e.g., *Obara*, 2002; *Gomberg et al.*, 2008], the relocation technique [*Shelly et al.*, 2006], and the Source Scanning Algorithm (SSA) [*Kao et al.*, 2005]. A limitation of these methods is that they are based on only a part of the signal, such as direct arrival for the SSA. In one instance a temporary seismic array was placed over the source of tremor and S minus P arrivals were used to find the hypocentral location [*La Rocca et al.*, 2009]. No generally applicable, robust method for tremor location currently exists. Time reversal is a promising method as it only requires having synchronized recorded waveforms. Its application to locate volcanic tremor has been examined in a recent 2D synthetic study [*Lokmer et al.*, 2009].

[3] Time reversal has been shown to be robust in locating time local sources in the laboratory [e.g., *Anderson et al.*, 2008; *Griffa et al.*, 2008; *Anderson et al.*, 2009a; *Ulrich et al.*, 2007, 2008b] as well as in the Earth [*Larmat et al.*, 2006, 2008]. Further, in a bounded, homogeneous, isotropic laboratory sample a continuous-wave source was located by time-reversing a set of detected steady state signals [*Anderson et al.*, 2009a].

[4] To extend time reversal from laboratory to Earth requires re-broadcasting full waveforms in a realistic computational model. We must deal with conditions that include: (1) poor and possibly asymmetric (about source) station coverage, (2) limited model volume and signal duration (3) a complex velocity model featuring low and high velocity zones. In a first study *Larmat and Johnson* [2008] located a synthetic tremor source in a realistic Earth/station set model. This investigation brought to the fore the importance of the appropriate choice of imaging fields, the aspect of the source location problem that is developed in this letter.

2. System Studied and Method of Study

[5] The study volume is a 250 km (E–W) × 190 km (S–N) × 60 km (vertical) portion of Southern California surrounding the San Jacinto segment of the San Andreas fault (Figure 1a). Local topography of the surface, basement and Mohorovičić discontinuities are considered. The 3D variation of the velocity parameters (shear velocity from 0.8 km/s to 4.5 km/s) are from the Southern Californian Velocity Model of *Süss and Shaw* [2003]. About 120 stations, from the University of California (Anza) and the California Institute of Technology (CI) networks are used (except Figure 4). The source time function [$s(t) = 0$ for $t < 0$ or $t > 150$; $\sin(\frac{2\pi t}{2*150}) \sum_{f_i} \cos(2\pi f_i t)$ for $0 \geq t \geq 150$, with $\{f_i\} = \{0.16; 0.23; 0.30$ Hz$\}$] is turned on at $t = 0$ and the forward propagation is followed out to time $T = 450$ s. The displacement field is recorded for $0 \leq t \leq T$, time reversed and re-broadcast (Figure S1).[3] Re-broadcast is followed out to time $2T$ with a clock that starts at $t_R = T - 75$ and passes through $t_R = 0$ at the time center of $s(t)$. Forward and time reversed propagation are based on the spectral element package SPECFEM3D [*Komatitsch et al.*, 2002]. The total number of elements in the study volume, 168,192, giving a time resolution of 3 s (CFL condition), corresponds to $>10^7$ grid points. We use 1,000 CPU-hrs on a Beowulf cluster consisting of 30 SMP with 2 dual-cores AMD Opteron 2216.

3. Imaging Fields

[6] Suppose data at a station set has been time reversed and re-broadcast into a velocity model as described above.

[1]Geophysics Group, Los Alamos National Laboratory, Los Alamos, New Mexico, USA.
[2]Department of Physics, University of Nevada, Reno, Nevada, USA.

0094-8276/09/2009GL040099$05.00

[3]Auxiliary materials are available in the HTML. doi:10.1029/2009GL040099.

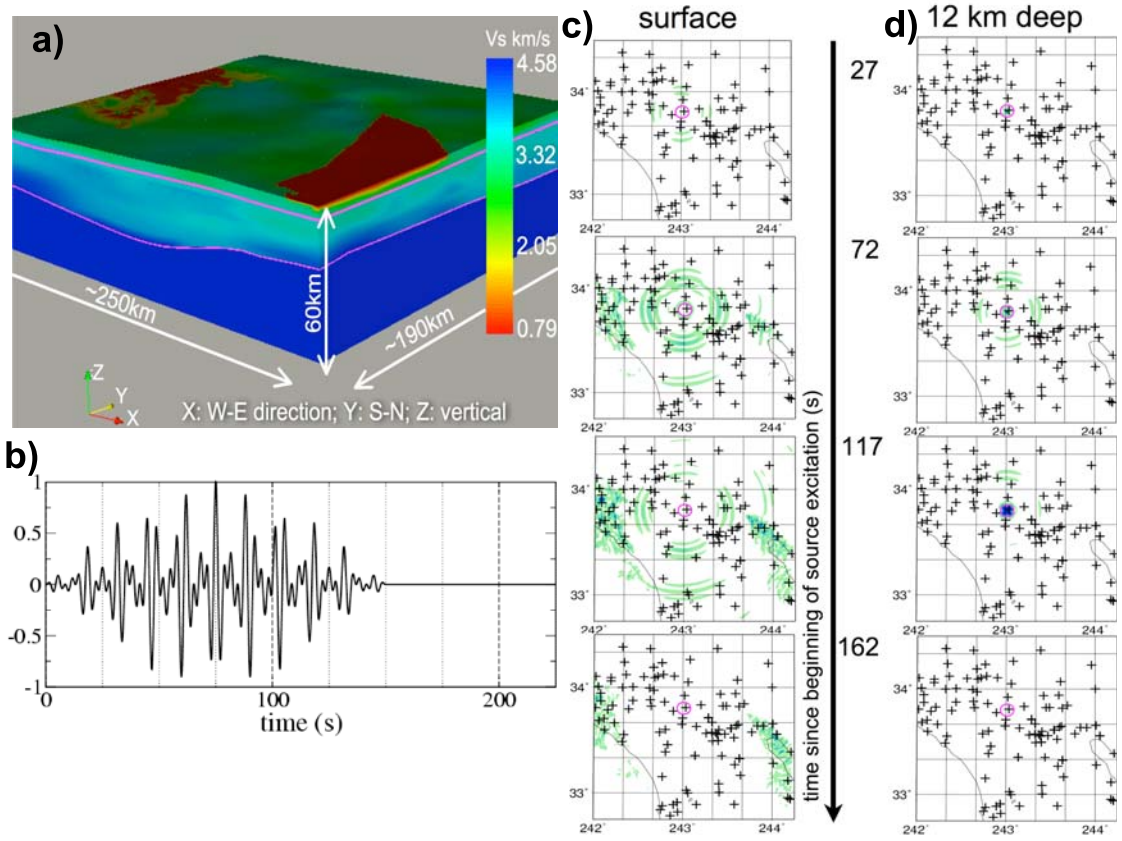

Figure 1. (a) The 3D velocity model of the study volume, centered on the San Jacinto segment of the San Andreas fault; co-ordinate system is at the lower left. (b) Long-lasting source time function ($s(t)$ in the text) applied with an horizontal strike-slip mechanism for the source. Snapshots of the norm of the displacement field, $B = |\mathbf{u}|$, (c) at the surface and (d) at source depth, 12 km. Note the accumulation of seismic energy on the surface in the two low velocity zones (shown in yellow in Figure 1a) corresponding to sedimentary basins on the East and West edges of the study volume.

From the resulting displacement field, $\mathbf{u}(\mathbf{x}, t)$, a picture of the source is to be constructed. We take $\mathbf{u}(\mathbf{x}, t)$ to be a continuous function of $\mathbf{x}$ and t and consider a set of imaging fields.

[7] 1. The brightness field, $B(\mathbf{x}, t)$, a scalar measure of the magnitude of $\mathbf{u}(\mathbf{x}, t)$, for example, $B(\mathbf{x}, t) = |\mathbf{u}(\mathbf{x}, t)|$, can be problematic in systems with large velocity contrast since $K(\mathbf{x}_1)u_1^2 \approx K(\mathbf{x}_2)u_2^2$ (energy conservation) could imply $u_1 \gg u_2$ for no other reason than $K(\mathbf{x}_1) \ll K(\mathbf{x}_2)$.

[8] 2. The divergence field, $D(\mathbf{x}, t)$, is a detector of displacement fields having compression/tension character, for example, P-waves. (See the end of the discussion of $\epsilon_{\mu\neq\nu}(\mathbf{x}, t)$ below.)

[9] 3. In contrast to D, the curl field, $\mathbf{C}(\mathbf{x}, t) = \nabla \times \mathbf{u}$, is a detector of shear character, for example, S-waves.

[10] 4. For the off diagonal strain field, $\epsilon_{\mu\neq\nu}(\mathbf{x}, t)$, source representation [*Aki and Richards*, 2002] and application of the adjoint method to source location [*Liu et al.*, 2004; *Tromp et al.*, 2005, 2008] demonstrate the association between each double couple in the moment tensor and a corresponding component of the strain tensor: $\epsilon_{xy} \leftrightarrow M_{xy}$. The 3 parts of the D field, $\epsilon_{\nu\nu}$, $\nu = x, y, z$, are associated with diagonal couples, $M_{\nu\nu}$.

[11] 5. For the energy flux, $Q_\nu(\mathbf{x}, t)$, the displacement field in an isotropic solid has energy current density (units $E/L^2/T$) [*Fetter and Walecka*, 1980]

$$(\mathbf{J}_3)_i = -\lambda\nabla\cdot\mathbf{u}\frac{\partial u_i}{\partial t} - \mu\sum_{j=1}^{3}\left(\frac{\partial u_j}{\partial x_i} + \frac{\partial u_i}{\partial x_j}\right)\frac{\partial u_j}{\partial t}, \tag{1}$$

$$= -\left(\lambda\nabla\cdot\mathbf{u} + 2\mu\frac{\partial u_i}{\partial x_i}\right)\frac{\partial u_i}{\partial t} - \mu\sum_{j\neq i}\left(\frac{\partial u_j}{\partial x_i} + \frac{\partial u_i}{\partial x_j}\right)\frac{\partial u_j}{\partial t}, \tag{2}$$

where the second line exhibits the energy current density in two parts, $(\mathbf{J}_3)_i^p$ carries compressive energy and $(\mathbf{J}_3)_i^s$ carries shear energy. A scalar measure of the energy current is provided by $\nabla \cdot \mathbf{J}_3$ or the energy flux found upon integrating $\nabla \cdot \mathbf{J}_3$ over a differentially small volume. See *Anderson et al.* [2009b] and P.-Y. Le Bas et al. (Probing the interior of a solid volume with time reversal and nonlinear elastic wave spectroscopy, submitted to *Physical Review Letters*, 2009) for application of this imaging field to laboratory data.

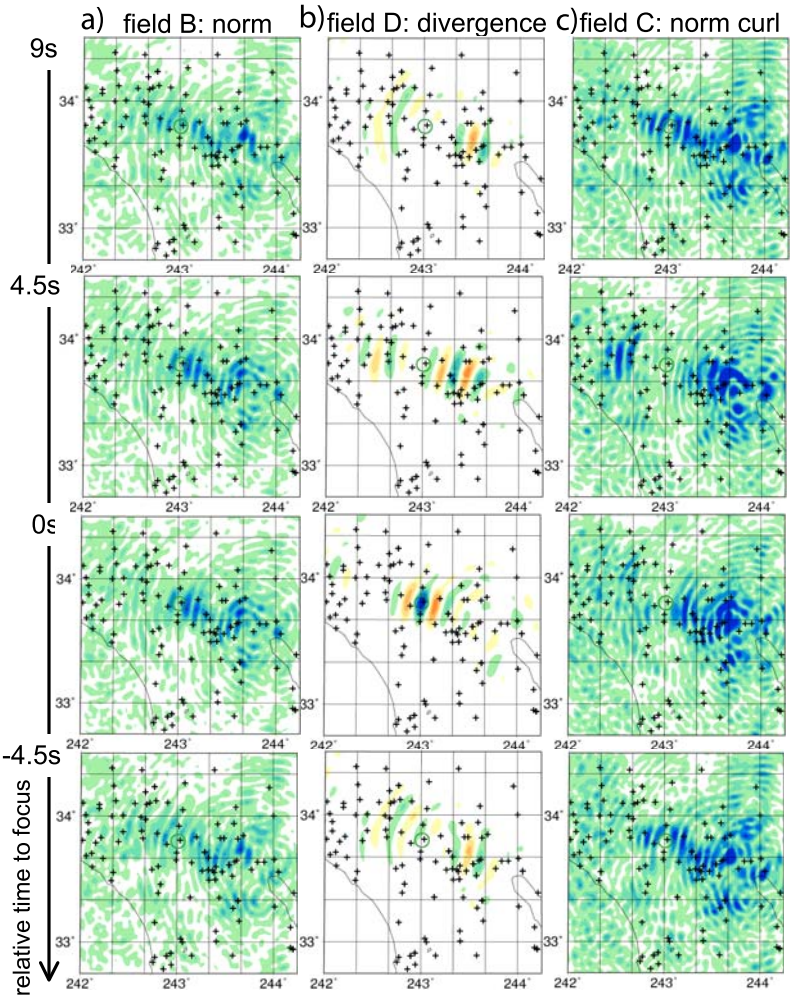

Figure 2. Time-reversal imaging of an isotropic source placed at z = 12 km, $M_{xx} = M_{yy} = M_{zz}$ and all off-diagonal M set to zero. Time $t_R = 0$ corresponds to the time of focus of the center of $s(t)$. (a) B, (b) D and (c) $C = \sqrt{\mathbf{C} \cdot \mathbf{C}}$ in the z = 12 km plane. There is no evidence of focusing with the B field (possibly expected to exhibit focus) or the C field (not expected to exhibit focus). There is excellent focusing with the D field as expected.

[12] The progression from B to Q is in the sophistication of the question being asked of the displacement field in forming an image to be examined for source location.

4. Results

4.1. Strong Influence of the Surficial Low Velocity Zones

[13] Figures 1c and 1d display the first 162 s of forward broadcast from a strike-slip source at z = 12 km ($M_{xy} \neq 0$ and all other M set to zero) using the B field. What is seen on the surface (Figure 1c) is in marked contrast to what is seen at source depth (Figure 1d). On reaching the surface near the east and west edges of the study volume the broadcast excites the low velocity zones (sedimentary basins $\leq$ 1 km deep) to large amplitude. These amplitudes induce a strong E–W dominance in the time reversed wavefield (called the E–W anisotropy; Figure S4).

4.2. Imaging Field

[14] For an isotropic source ($M_{xx} = M_{yy} = M_{zz}$ and all other M set to zero) at 12 km depth we detect the displacement field time trains at the surface stations, time reverse and re-broadcast them into the interior. We use the B field as an imaging field, Figure 2 (left). The B field fails to give a single focus point; the edges of the low velocity zone appear as maxima of B comparable to that at the known source point. However the D field (middle column), sympathetic to the source, displays a progressive convergence onto the source point from t_R = +9.0 s to t_R = 0 s before diverging from it. The C field, a detector of shear waves, images the low-velocity zone, indicating P to S conversion in that area. The snapshots also show strong evidence of the E–W anisotropy of the time reversed broadcast.

[15] In Figure 3 we show the time-reversed broadcast of a strike-slip source at z = 12 km ($M_{xy} \neq 0$ and all other M set to zero) The fields B, D and ϵ_{xy} are shown in the source plane. The B field shows a local maximum at $t_R = 0$ but the converging/diverging behavior is just above the noise level. The ϵ_{xy} field, sympathetic to the source, converges to the source location and then diverges away from it. Superposed on this focusing is strong evidence of the E–W anisotropy of the time reversed broadcast. Figure S2 shows the result for C that displays a weak focus at the source point. For an

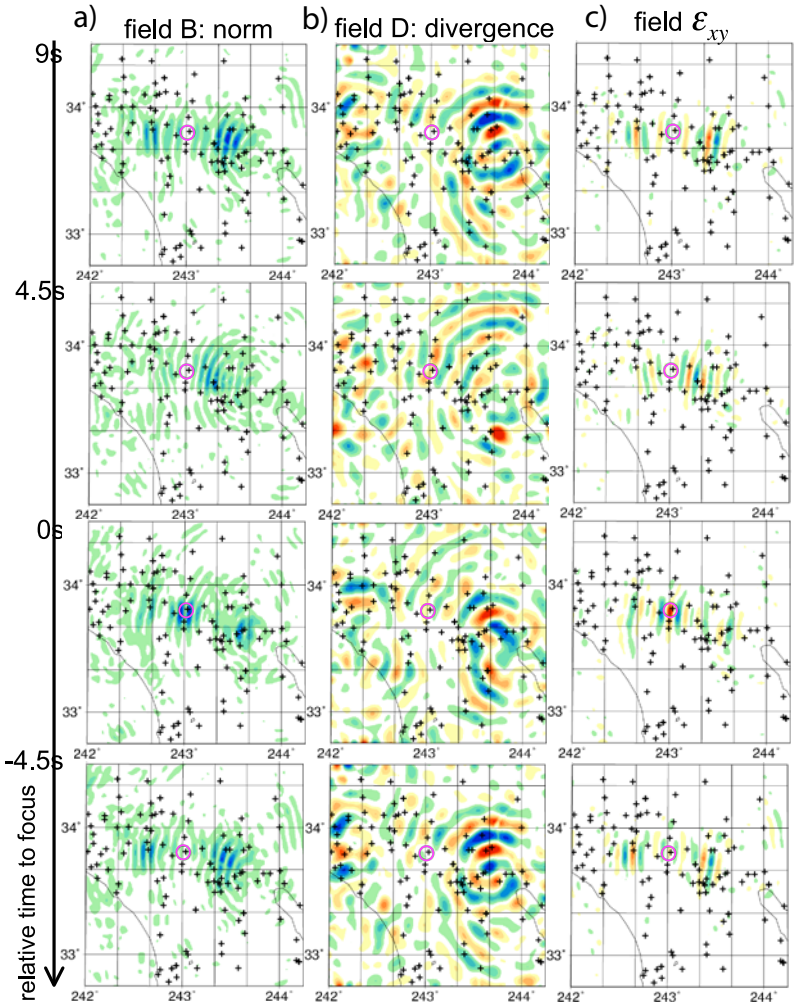

Figure 3. Time-reversal imaging of a shear-like source placed at z = 12 km, $M_{xy} \neq 0$ and all other M set to zero. Time t_R = 0 corresponds to the time of focus of the center of $s(t)$. (a) B, (b) D and (c) ϵ_{xy} in the z = 12 km plane. There is no evidence of focusing with the B field (possibly expected to exhibit focus) or the D field (not expected to exhibit focus). Focusing appears on the image obtained with the xy component of the strain as expected.

isotropic re-broadcast the C_z field (or equivalently the C field) would be a poor detector of the source (for which $M_{xy} = M_{yx}$) as one would have $\partial u_x \partial y \approx \partial u_y \partial x$ or $C_z = \partial u_x \partial y - \partial u_y \partial x \approx 0$. Because of the anisotropy of the re-broadcast $\partial u_x/\partial y$ and $\partial u_y/\partial x$ are unbalanced, the C_z field also focuses. These observations suggest that while the ϵ_{xy} field is prompted by our a priori knowledge, both this field and the C_z field combine to provide a deeper understanding of the source and of the volume in which the re-broadcast is propagating.

4.3. Deep Source (30 km)

[16] The fields B, D, C and ϵ_{xy} are shown in the source plane at the time t_R = 0 in Figure S3 for a strike-slip source ($M_{xy} \neq 0$ and all other M set to zero) at z = 30 km. The B, C and ϵ_{xy} fields, sensitive to shear components of the wave-field, display similar focusing. Two features of propagation contribute to this result. First, the z = 30 km source is much deeper than the near-surface sedimentary basins. Second, the 30 km deep source is within a local deep low velocity zone (corresponding to the deflection of the Moho beneath the coastal Range).

4.4. Role of the Station Distribution

[17] In Figure 4, we show the ϵ_{xy} field, for the time reversed broadcast for a strike-slip source at z = 30 km, for the same realistic station set used throughout the paper (left column) and for a dense, uniformly spaced station set (right column). The snapshots, made at the time t_R = 0, show focusing strongly marked by the E–W anisotropy. The unbalanced distribution of incident energy (primarily coming from the edge of the East low velocity zone, see Animations S1–S4) creates an elongated focus in the N–S direction and causes a slight offset from the original source point.

[18] The most striking observation from Figure 4 is that the two time reversed broadcasts display very similar features, with only an increase in amplitude when more stations are used for the broadcast. Thus a limited and realistic array of stations can give a proper source location.

5. Discussion and Conclusions

[19] We computed 3D time reversed elastic wave propagation with a realistic velocity model and station set for the

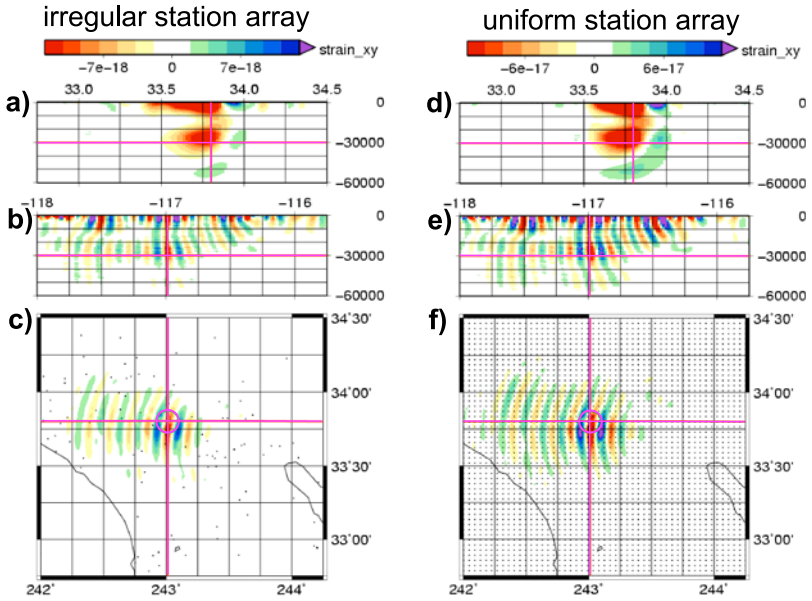

Figure 4. Time-reversal imaging of a shear-like source placed at z = 30 km, $M_{xy} \neq 0$ and all other M set to zero. (left) Station set used in Figures 1–3 and (right) a dense, evenly spaced station set. The imaging field is the xy component of the strain field at time $t_R = 0$ displayed on the (a, d) S–N and (b, e) E–W planes that cross at the source location and (c, f) on the horizontal plane at source depth. The surface location of the stations are shown as black dots. The images obtained in the two cases are remarkably similar.

volume surrounding the San Jacinto segment of the San Andreas fault. We have introduced and examined the merits of different imaging fields for application to long lived sources. We have demonstrated the need to use imaging fields sympathetic to the source type. This is especially true for a source located relatively close to the surface or in close proximity to low velocity zones, which act as seismic energy magnets. The correct choice of imaging field has a precise answer in the adjoint form of the source location problem. This sharp connection is smeared in the presence of a realistic velocity model/station set.

[20] We found, looking at station set distribution, that a limited, realistic array of stations gives a satisfactory time-reversal source location. This result suggests that the primary factors affecting focusing quality are: (1) the presence of strong contrast in the velocity model and (2) limitations of aperture that cannot be compensated for by a dense station set.

[21] An advantage of working with different imaging fields is that besides location, they allow characterization of the spatial structure of a source. A combination of different imaging fields provides a deeper understanding of the source and of the volume in which the re-broadcast is propagating.

[22] Strong imbalance of the characteristics of the time-reversed wavefield can degrade the quality of the source location, for example, the E–W anisotropy of the time-reversed broadcast for the 30 km deep source. This prompts the use of other imaging fields (the energy current density [*Anderson et al.*, 2009b]), the use of space-time correlations [*Ulrich et al.*, 2008a] or the use of fields based on time evolution, suggested by time-reversed animations. In addition to more sophisticated choices of imaging fields, there are various tessellations [*Larmat et al.*, 2006] and station weight schemes may be applied. These refinements offer the possibility of further improvement in source location and reconstruction.

[23] **Acknowledgments.** This work was supported by Institutional Support (LDRD) at Los Alamos National Laboratory.

References

Aki, K., and P. G. Richards (2002), *Quantitative Seismology*, Univ. Sci. Book, Sausalita, Calif.

Anderson, B. E., M. Griffa, C. Larmat, T. J. Ulrich, and P. A. Johnson (2008), Time reversal, *Acoust. Today*, *4*, 5–16.

Anderson, B. E., R. A. Guyer, and T. J. Ulrich (2009a), Time reversal of continuous-wave, steady-state signals in elastic media, *Appl. Phys. Lett.*, *94*, 111908, doi:10.1063/1.3097811.

Anderson, B. E., R. A. Guyer, T. J. Ulrich, P.-Y. Le Bas, C. Larmat, M. Griffa, and P. A. Johnson (2009b), Energy current imaging method for time reversal in elastic media, *Appl. Phys. Lett.*, *95*, 021907, doi:10.1063/1.3180811.

Fetter, A., and J. Walecka (1980), *Theoretical Mechanics of Particles and Continua*, McGraw-Hill, New York.

Gomberg, J., J. L. Rubinstein, Z. Peng, K. C. Creager, J. E. Vidale, and P. Bodin (2008), Widespread triggering of nonvolcanic tremor in California, *Science*, *319*, 173, doi:10.1126/science.1149164.

Griffa, M., B. E. Anderson, R. A. Guyer, and T. J. Ulrich (2008), Investigation of the robustness of time reversal acoustics in solid media through the reconstruction of temporally symmetric sources, *J. Phys. D Appl. Phys.*, *41*, 085415, doi:10.1088/0022-3727/41/8/085415.

Kao, H., S. Shan, H. Dragert, and G. Rogers (2005), A wide depth distribution of seismic tremors along the northern Cascadia margin, *Nature*, *436*, 841–844, doi:0.1038/nature03903.

Komatitsch, D., J. Ritsema, and J. Tromp (2002), The spectral-element method, Beowulf computing, and global seismology, *Science*, *298*, 1737–1742, doi:10.1126/science.1076024.

Larmat, C., and P. A. Johnson (2008), Time reversal location of non-volcanic tremor in California, *Eos Trans. AGU*, *89*(53), Fall Meet. Suppl., Abstract U33A-0049.

Larmat, C., J.-P. Montagner, M. Fink, Y. Capdeville, A. Tourin, and E. Clévédé (2006), Time-reversal imaging of seismic sources and application to the great Sumatra earthquake, *Geophys. Res. Lett.*, *33*, L19312, doi:10.1029/2006GL026336.

Larmat, C., J. Tromp, Q. Liu, and J.-P. Montagner (2008), Time reversal location of glacial earthquakes, *J. Geophys. Res.*, *113*, B09314, doi:10.1029/2008JB005607.

La Rocca, M., K. C. Creager, D. Galluzzo, S. Malone, J. E. Vidale, J. R. Sweet, and A. G. Wech (2009), Cascadia tremor located near plate interface constrained by *S* minus *P* wave times, *Science*, *323*, 620–623, doi:10.1126/science.1167112.

Liu, Q., J. Polet, D. Komatitsch, and J. Tromp (2004), Spectral-element moment tensor inversions for earthquakes in southern California, *Bull. Seismol. Soc. Am.*, *94*, 1748–1761, doi:10.1785/012004038.

Lokmer, I., G. S. O'Brien, D. Stich, and C. Bean (2009), Time reversal imaging of synthetic volcanic tremor sources, *Geophys. Res. Lett.*, *36*, L12308, doi:10.1029/2009GL038178.

Obara, K. (2002), Nonvolcanic deep tremor associated with subduction in southwest Japan, *Science*, *296*, 1679–1681, doi:10.1126/science.1070378.

Shelly, D. R., G. C. Beroza, S. Ide, and S. Nakamula (2006), Low-frequency earthquakes in Shikoku, Japan, and their relationship to episodic tremor and slip, *Nature*, *442*, 188–191, doi:10.1038/nature04931.

Süss, M., and J. Shaw (2003), *P* wave seismic velocity structure derived from sonic logs and industry reflection data in the Los Angeles basin, California, *J. Geophys. Res.*, *108*(B3), 2170, doi:10.1029/2001JB001628.

Tromp, J., C. Tape, and Q. Liu (2005), Seismic tomography, adjoint methods, time reversal and banana-doughnut kernels, *Geophys. J. Int.*, *160*, 195–216.

Tromp, J., D. Komatitsch, and Q. Liu (2008), Spectral-element and adjoint methods in seismology, *Commun. Comput. Phys.*, *3*, 1–32.

Ulrich, T. J., P. A. Johnson, and R. A. Guyer (2007), Interactions dynamics of elastic waves with a complex nonlinear scatterer through the use of a time reversal mirror, *Phys. Rev. Lett.*, *98*, 104301, doi:10.1103/PhysRevLett.98.104301.

Ulrich, T. J., M. Griffa, and B. E. Anderson (2008a), Symmetry-based imaging condition in time reversed acoustics, *J. Appl. Phys.*, *104*, 064912, doi:10.1063/1.2980323.

Ulrich, T. J., A. Sutin, R. A. Guyer, and P. A. Johnson (2008b), Time reversal and non-linear elastic wave spectroscopy (tr news) techniques, *Int. J. Non Linear Mech.*, *43*, 209–216, doi:0.1016/j.ijnonlinmec.2007.12.017.

R. A. Guyer, P. A. Johnson, and C. S. Larmat, Geophysics Group, EES-17, Los Alamos National Laboratory, Los Alamos, NM 87544, USA. (carene@lanl.gov)